Clays and Clay Minerals, Vol. 61, No. 4, 361–374, 2013.

KINETICS OF DESORPTION OF WATER, ETHANOL, ETHYL ACETATE, AND TOLUENE FROM A MONTMORILLONITE

Pascal Clausen[1,*], Lorenz Meier[2], Eric Hughes[3], Christopher J. G. Plummer[1], and Jan-Anders E. Månson[1]

[1] Laboratoire de Technologie des Composites et Polymères (LTC), Ecole Polytechnique Fédérale de Lausanne (EPFL), CH-1015 Lausanne, Switzerland
[2] Riedtlistrasse 67, 8006 Zurich, Switzerland
[3] Nestlé Research Center, Ver-Chez-Les-Blanc, 1000 Lausanne 26, Switzerland

Abstract—Desorption processes of low-molecular-weight compounds from the surface of smectites into the gas phase determine a number of processes, *e.g.* those involved in drug delivery and the release of herbicides. The desorption has not been investigated thoroughly and is not well understood. The present study was undertaken in order to understand better the factors influencing these desorption mechanisms. Starting with a very pure standard (Na^+-rich) montmorillonite (Kunipia-F), which was exchanged against cations with different hydration properties (Ca^{2+}, Li^+, phenyltrimethylammonium, hexyltrimethylammonium), the experiments explored the rate of desorption of volatiles with different chemical functionalities (water, ethanol, ethyl acetate, and toluene). The desorption was monitored by thermogravimetry and differential scanning calorimetry under isothermal conditions, and by ramping the temperature at a constant rate. The experiments were compared with numerical calculations based on finite-element methods and with analytical models. These data point to a two-step mechanism where the desorption follows the curve of the equilibrium desorption isotherms of those molecules on the montmorillonite. The bulk-like volatiles (*i.e.* volatiles with release kinetics close to that of the bulk liquids) were desorbed in a first step. With a decrease in the degree of coverage of the volatile on the montmorillonite, the desorption was increasingly dominated by the strength of interaction between the volatile and the interlayer cations of the montmorillonite.

Key Words—Desorption, Ethanol, Equilibrium Sorption Isotherm, Ethyl Acetate, Ion Exchange, Modeling, Montmorillonite, Numerical Method, Release, Smectite, Toluene, Volatile, Water.

INTRODUCTION

The well defined desorption of molecules can be used to maintain a constant supply of active components crucial for applications in drug delivery, food, herbicides, cosmetics, construction, or environmental purposes (El-Nokaly *et al.*, 1993). The development of methods and tools allowing the quantitative prediction of desorption from solid surfaces can have a marked impact on the design, performance, and applicability in these areas. The present study focused on the layered silicate, montmorillonite, with its very large specific surface area of ~600 m^2/g to adsorb a variety of substances representing standard chemical functionalities in order to understand and predict the desorption behavior.

Previous investigations aiming to predict the rates of desorption of volatiles proposed various approaches: phenomenological models (Grismer, 1987a, 1987b), analytical solutions expected from transport models (Veith *et al.*, 2004; Morrissey and Grismer, 1999; Siepmann *et al.*, 1998), statistical physics (Frezzotti *et al.*, 2005), statistical rate theory (Ward and Fang, 1999), general rate laws (Bray and Redfern, 1999), and numerical simulations (Girard *et al.*, 2006; Fujii *et al.*, 2003; Keyes and Silicox, 1994). A few studies have been devoted to the desorption kinetics of volatiles from smectites to the gas phase (Shih and Wu, 2004; Chang *et al.*, 2003; Bray and Redfern, 1999; Keyes and Silicox, 1994; Arocha *et al.*, 1996; Siepmann *et al.*, 1998; Steinberg *et al.*, 1994).

Previously presented data measured the rate of desorption of water from granular (Na^+-rich) montmorillonite (Clausen *et al.*, 2011). Due to the special design of their experimental apparatus, this rate of desorption in their experimental setup could be related reliably to the equilibrium desorption isotherm while the influences from effective diffusion (*i.e.* diffusion other than interlayer diffusion) effects inside the sample were minor. Further evidence of the relation between the equilibrium desorption isotherms and the rate of de-sorption was provided by correlating the enthalpy of vaporization with the rate of desorption. The determined enthalpy of vaporization of water desorbed from (Na^+-rich) montmorillonite granules as a function of the water coverage showed step transitions at ~44, 46, and 49 kJ/mol. These steps corresponded to those in the equilibrium desorption isotherm. The measurements were compared with numerical calculations of the rate of desorption. The authors used the local gas-phase concentration of water at the

* E-mail address of corresponding author:
pascalclausen@hotmail.com
DOI: 10.1346/CCMN.2013.0610414

montmorillonite surface as input data in their numerical model. This gas phase concentration was a function of the coverage of water on the montmorillonite surface, given by the desorption branch of the equilibrium sorption isotherm. The numerical calculations explained the influence of the equilibrium desorption isotherm on the rate of desorption.

The equilibrium sorption isotherms of small inorganic cations (*e.g.* Na^+, K^+, Li^+, Ca^{2+}) on smectites have been studied by experimental measurements (Ferrage *et al.*, 2005; Tamura *et al.*, 2000; Bérend *et al.*, 1995; Kraehenbuehl *et al.*, 1987; Norrish, 1954) and by molecular dynamics simulations (Tambach *et al.*, 2006; Hensen and Smit, 2002; Boek *et al.*, 1995). These equilibrium sorption isotherms depend heavily on the hydration energy of the interlayer cations. One feature of these isotherms is their characteristic stepwise sorption behavior. A semi-plateau observed at low water coverage is ascribed to a state where the interlayer cations are partially hydrated. In this state, the interlayer distance between the smectite platelets corresponds to one layer of water, and the interlayer cations are in direct contact with the smectite surface (inner-sphere surface complexes). The semi-plateau observed at intermediate water coverage is ascribed to a state where the interlayer cations are fully hydrated. In this state, the distance between the smectite platelets corresponds to two layers of water, and the interlayer cations are not in direct contact with the smectite surface (outer-sphere surface complexes). Some water sorbed in the smectite can be in a state where the water molecules are not coordinated to the interlayer cations (Salles *et al.*, 2008; Cases *et al.*, 1997). However, water is predominantly sorbed to the interlayer cations as a consequence of the greater sorption energy of inner- and outer-sphere surface complexes, so that the type of water is predominantly water coordinated to the interlayer cations. Indeed, at low and intermediate water coverages, the number of water molecules found per interlayer cation was the same as the expected coordination number of the interlayer cation (Clausen *et al.*, 2011; Michot *et al.*, 2005).

Effective diffusion coefficients for water in smectites have been published in the literature (Bourg *et al.*, 2006; Nakashima, 2006; Suzuki *et al.*, 2004; Nakashima, 2003; Sato and Suzuki, 2003; Nakashima, 2002; Nakashima, 2000a; Nakashima, 2000b; Duval *et al.*, 1999). Data are also available for the molecular diffusion coefficients of water in smectites with inorganic interlayer cations (Marry *et al.*, 2008; Malikova *et al.*, 2006; Skipper *et al.*, 2006; Swenson *et al.*, 2000; Chang *et al.*, 1995; Poinsignon *et al.*, 1989; Tuck *et al.*, 1984, 1985; Cebula *et al.*, 1981). To calculate the effective diffusion coefficient of water in smectites, simplified tortuosity models (Lusti *et al.*, 2004; Bharadwaj, 2001; Duval *et al.*, 1999) as well as multiscale calculations, including the interlamellar diffusion around stacks of platelets and the different porosity (Fujii *et al.*, 2003), were applied.

The present study focused on the measurements of the rate of desorption of volatiles from a montmorillonite using thermogravimetry and differential scanning calorimetry, combined with numerical calculations. Molecules with different chemical functionalities and polarities, such as water, ethanol, ethyl acetate, and toluene, were chosen as representative volatiles. Inorganic and organic interlayer cations with different hydration properties, such as Na^+, Li^+, Ca^{2+}, phenyltrimethylammonium, and hexyltrimethylammonium, were selected for the study.

The following measurements were performed: (1) equilibrium desorption isotherms of water on (Na^+-rich) montmorillonite, Ca^{2+}-exchanged montmorillonite, phenyltrimethylammonium-exchanged montmorillonite, and hexyltrimethylammonium-exchanged montmorillonite; (2) isothermal rate of desorption of water from the same ion-exchanged montmorillonite; (3) ramp-temperature measurements of the rate of desorption of different volatiles (water, ethanol, ethyl acetate, and toluene) from (Na^+-rich) montmorillonite and Li^+-exchanged montmorillonite; and (4) isothermal rate of desorption of volatiles (water, ethanol, ethyl acetate, and toluene) from the (Na^+-rich) montmorillonite. Numerical calculations of the rate of desorption were performed and compared with the experimental findings. The results provide a greater understanding of the influences of the equilibrium desorption isotherms on the rate of desorption, and a desorption mechanism is proposed.

EXPERIMENTAL METHODS AND MATERIALS

Materials

Montmorillonite. High-purity (Na^+-rich) montmorillonite was purchased as 'Kunipia-F' from Kunimine Industry Co. Ltd., Japan. The montmorillonite came from the Tukinuno Mine, Yamagata Prefecture, Japan, and is the <2 μm fraction of this montmorillonite-rich rock. During industrial processing of Kunipa-F, this fraction was dried at 140ºC according to Morodome and Kawamura (2009). Previous characterization of the montmorillonite showed that the material used for the present study was very pure montmorillonite with predominantly Na^+ interlayer cations (Clausen *et al.*, 2011; Ochs *et al.*, 2004; Sato and Suzuki, 2003). The measured cation exchange capacity (CEC) was 116 meq/100 g (data sheet: 115 meq/100 g) (www.kunimine.co.jp).

Salts. The salts used for the study were lithium chloride, calcium chloride, phenyltrimethylammonium chloride, and hexyltrimethylammonium chloride. All salts were obtained from Aldrich.

Volatiles. The model volatiles used for the experiments were deionized water (for chromatography, Merck), ethanol (absolute Guaranteed Reagent (GR) for analysis, Merck), ethyl acetate (GR for analysis, Merck), and toluene (GR for analysis, Merck).

https://doi.org/10.1346/CCMN.2013.0610414 Published online by Cambridge University Press

Measurement of the CEC

The CEC was determined following the standard procedure of Meier and Kahr (1998) using the layered silicate-selective copper II complex of triethylene tetramine. The montmorillonite was ultrasonicated for 2 min (Polytron, PT2100, 500 W, 50−60 Hz) and the measurement repeated three times using a UV/Vis Helios Unicam spectrometer. The mean CEC determined was 116 mmol/100 g (±2 mmol/100 g).

Organic cation-exchange of the montmorillonite

The (Na^+-rich) montmorillonite was homoionically exchanged with phenyltrimethylammonium (PHTMA) or hexyltrimethylammonium (HTMA) by ion exchange using a batch method (Polubesova *et al.*, 1997). Prior to the ion exchange, the montmorillonite powder was dried for 2 days at 60ºC under a vacuum of 90 mbar using a P_2O_5 adsorbent in order to quantify the dry weight of the montmorillonite. 1.00 g of the dried montmorillonite powder was dispersed in 100 mL of a 50% water/methanol solution by means of ultrasonic treatments of 5 min duration. The modifying cation salt was dissolved in 50 mL of a 50% water/methanol solution in a proportion of 1.4 times the molar amount of the determined CEC (116 meq/100 g). The organic cation solutions were transparent, indicating good solubility in the 50% methanolic solution. The ion-exchanged montmorillonite dispersion was diluted with a 50% water/methanol to give 300 mL of suspension. Subsequently, the organic cation solutions were added and the montmorillonite flocced immediately indicating ion exchange. The suspension was mixed for another 15 min with a high-performance shear mixer (Polytron PT2100, 500 W, 50-60Hz) and was stirred for 24 h at 60ºC. After centrifugation of the mixture (10 min, 700 × g), the supernatant was removed. After addition of 400 mL of methanol, the mixture was subjected to a 3 min treatment with the shear mixer. The mixture was centrifuged again and the supernatant removed. This washing procedure was repeated once with methanol and twice with ethanol, after which the ion-exchanged montmorillonite was dried at room temperature. This exchange procedure process was repeated twice. With this procedure, the remaining amount of Na interlayer cations in the ion-exchange montmorillonite can be reasonably assumed to be <10%.

Cation exchange of the montmorillonite: inorganic cations (Na^+-rich) montmorillonite. The (Na^+-rich) montmorillonite Kunipia-F was used without further purification.

Ca^{2+}-exchanged montmorillonite. For Ca^{2+}-exchanged montmorillonite, an exchange procedure similar to the organic-cation-modification procedure was used, except bidistilled water was used here as the washing solution rather than the methanol/water solution.

Li^+-exchanged montmorillonite. The Li^+-exchanged montmorillonite was achieved in a column ion-exchange setup. Dried montmorillonite granulates (40 g) of 2 mm grain size were loosely packed into a glass tube closed at one end with a stopcock. An aqueous solution of 15 wt.% lithium chloride (~4 mol/L) was added. The ion exchange was performed by flow through the column at a flow rate of 2 L per day for 5 days, corresponding to a CEC (116 meq/100 g)-related excess of ~760. The Li^+-exchanged montmorillonite was washed with ethanol at 2 L per day for 5 days and then allowed to dry in a fume hood.

Interlayerdistance with different interlayer cations

The interlayer distance of the ion-exchanged montmorillonite was measured by X-ray diffraction (XRD) using a Siemens Kristalloflex 805 diffractometer (Munich, Germany) (λ = 1.5418 Å) from oriented films. The montmorillonite films used for XRD measurements were achieved by dropping 1 wt.% montmorillonite dispersions onto 1 cm-diameter low-density polyethylene substrates The measurements ranged from 3.5º to 8.5º2θ with a step angle of 0.02º2θ and a time per step of 3 s. The antiscattering slit was 1 mm, the divergence slit was 1 mm, and the detector slit was 0.05 mm. Samples were measured by XRD immediately after removal from the desiccator but they were not protected from the atmosphere during the measurement. By restraining the measurement range to a narrow region, the rehydration effects were minimized. For this reason, differences in layer-to-layer distances should reflect differences in the type of intercalating cation. The difference between the layer-to-layer distances, d_{001}, of the unmodified montmorillonite and that of the ion-exchanged montmorillonite refers to the presence of the intercalating cations in the montmorillonite (Table 1).

Verification of completion of Na^+-cation exchange

Nuclear magnetic resonance (NMR) was used to confirm the complete removal of Na^+ as the exchanged cation. All NMR experiments were performed on a Bruker DSX Avance wide-bore NMR spectrometer (Rheinstetten, Germany). The proton Larmor frequency

Table 1. Interlayer distances (d_{001}) of the ion-exchanged montmorillonite measured at room temperature and ambient relative humidity. Prior to the experiments, the samples were dried for 2 days at 60ºC at 90 mbar in the presence of a P_2O_5 adsorbent.

Organic cation	d_{001} (nm)
Ca^{2+}	1.46
Na^+	1.22
PHTMA	1.46
HTMA	1.37

https://doi.org/10.1346/CCMN.2013.0610414 Published online by Cambridge University Press

was 400.13 MHz (9.4 T). A triple resonance 4 mm magic angle spinning probe was used.

Montmorillonite samples were spun at 8 kHz. ^{23}Na NMR single-pulse experiments were run for the exchanged montmorillonite. The measurement conditions were kept the same for all NMR experiments. The spectral width was 200 kHz; 8192 complex points were taken of the free induction decay. The time domain signal was smoothed using an exponential filter of 20 Hz; the time domain signal was increased to 16 k points by adding zeros to the end of the data set and then Fourier transformed. The 90º pulse width was 4.5 µs, and 1024 transients were acquired with a recycle delay of 1 s.

A calibration curve was obtained by recording spectra of static samples of NaCl solutions ranging in concentration from 3.2×10^{-3} to 3.2×10^{-6} mol/cm^3. Using this calibration curve, the NMR spectra of the (Na^+-rich) montmorillonite was found to correspond to a concentration of 2.5×10^{-6} mol/cm^3 (signal to noise ratio = 62.6). The spectra of the ion-exchanged montmorillonite were almost flat. The low Na^+-signal indicated the residual amounts of Na^+ interlayer cations in the ion-exchanged montmorillonite to be <10% as determined by reference measurements.

Determination of equilibrium desorption isotherms

The montmorillonite equilibrium desorption isotherms of water were measured by differential thermogravimetry using a Dynamic Vapor Sorption (DVS) instrument from Surface Measurement Systems, UK.

The general procedure for sorption equilibria included using 15−30 mg of montmorillonite in every measurement. The samples were placed in glass crucibles (~1 cm in diameter) and equilibrated at relative humidities (RH) between 95% and 0% in steps of 5%. In order to regulate the RH, dry nitrogen gas (99.995% purity) was mixed in appropriate ratios with the same gas equilibrated with the relative humidities over saturated salt solutions of NaCl, $MgCl_2$, and LiCl at 25ºC and 35ºC. The equilibrium was reached when weight variations remained below 0.002% for a period of 10 min.

The desorption isotherms of the organic compounds (ethanol, ethyl acetate, and toluene) were performed with a DVS-Advantage instrument (Surface Measurements Systems, UK). The partial pressure of the organic compound was adjusted by bubbling dry carrier gas at prescribed flow rates (dried air, cleaned with an adsorption filter; H_2O concentration <15 ppb) through bottles containing the organic liquid. The partial pressure of the organic pressure was measured with a built-in dew point analyzer. 15- to 30-mg samples of montmorillonite were equilibrated at relative partial pressures ranging from ~90% down to 0%. Montmorillonite samples were regarded as being equilibrated when the weight did not vary by more than 0.01% for 10 min.

The water-equilibrium sorption isotherms are often expressed as the water coverage in the montmorillonite, θ, as a function of the water activity, a_w, defined as the ratio between the actual equilibrium vapor pressure, p, and the saturated vapor pressure of water, p_s. In what follows, a_w was converted into the gas-phase concentration, c, *via* equation 1. θ was computed as the number of water molecules sorbed per unit cell of the montmorillonite.

$$c = \frac{p}{kT} = a_w \frac{p_s}{kT} \quad (1)$$

$$\theta = w_f \frac{M_{w_w}^{mmt}}{M_{w_w}^{water}} \quad (2)$$

where k is the Boltzmann constant, w_f is the weight fraction of water on the montmorillonite sample, M_w^{mmt} is the molar mass of the montmorillonite unit cell (746 g/mol (Clausen *et al.*, 2011)), and M_w^{water} is the molecular weight of water.

Measurement of the rate of desorption

The rates of desorption of the volatiles were determined by thermogravimetry (TG) and 3D differential scanning calorimetry (DSC) using a commercial Sensys TG-DSC instrument from Setaram, France. Aluminum crucibles 5 mm in diameter and 10 mm high were used as sample holders. The sample and reference crucibles were placed at the center of each of the two 7 mm-diameter columns of the thermostated DSC chamber. The crucibles were subjected to a dry nitrogen carrier gas flow ranging from 5 mL/min to 100 mL/min per column. In order to minimize pollution by external air inside the instrumentation during sample loading, the chamber was handled in a slight overpressured polyethylene bag containing a continuous flow of dry nitrogen gas (99.9995% pure).

The measurements were performed under isothermal conditions at 25ºC and 35ºC ±0.1ºC, and at temperatures ranging from 23ºC to 200ºC. The scanning rate was 2ºC/min. Duplicate measurements were performed for each type of volatile and each type of ion-exchanged montmorillonite, with high reproducibility.

General preparation of samples

Cylindrical samples 4.3 mm in diameter and 2 mm high were prepared in molds of the same dimension using montmorillonite slurries. Prior to the desorption measurements, the samples were first dried for 2 days at 60ºC under a vacuum of 90 mbar over P_2O_5 giving a typical final sample weight of the order of 25 mg. For the isothermal desorption measurements, these samples were then equilibrated for 7 days at solvent-relative vapor pressures >95% using mixtures of dry and saturated flows. For the temperature scans, cylindrical samples were first stored in the thermogravimetric

https://doi.org/10.1346/CCMN.2013.0610414 Published online by Cambridge University Press

apparatus for 1 night in a dry nitrogen carrier gas flow and a temperature of 50ºC. Then, 5 μL droplets of the volatile liquids were deposited on the cylindrical samples. A fresh montmorillonite sample was used for each experiment.

Numerical simulations for the isothermal rate of desorption

The procedure for numerical calculations of the isothermal rate of desorption was described in detail in a previous study (Clausen *et al.*, 2011). The geometrical model constructed for the numerical calculations is a close approximation to the real Sensys instrumentation: a cylindrical column 7 mm in diameter and 100 mm high with a cylindrical crucible 5 mm in diameter and 10 mm high at its center with the sample at the bottom of the crucible.

Standard equations to describe fluid behaviors were used to model the desorption process (Navier, 1822; Landau and Lifschitz, 1987). The resulting system of equations was solved by finite-element methods in 2D cylindrical coordinates using the COMSOL software package (www.comsol.com). No additional routine was implemented. The inputs used by the software were the equations for the conservation of momentum (Navier-Stokes equation), the conservation of mass (continuity equation), the diffusion-convection equation, the equation of state (equilibrium desorption isotherm), and the material parameters included in those equations.

Equation of state. The local gas-phase concentration, c, in the vicinity of the sample surface was assumed to be in instantaneous equilibrium with the local volatile coverage θ sorbed on the sample surface. This assumption provides an equation of state given by the curve of the equilibrium desorption isotherm of the volatiles on the montmorillonite.

Boundary conditions. The initial value of c for the volatiles was set to zero. A constant flux was prescribed at the top of the cylindrical column in order to simulate the carrier-gas flow, and the pressure measured in the instrumentation was prescribed at the bottom of that column. No-slip (zero-velocity) boundary conditions were prescribed at the sample surface and slip (sliding) boundary conditions were prescribed at the walls of the crucible and the column.

Table 2. Vapor pressures of the volatiles.

Chemical species	Temperature (ºC)	Saturated vapor pressure (Pa)
Water	25	3167
Water	35	5624
Ethanol	35	13757
Ethyl acetate	35	20119
Toluene	35	6239

Material parameters. To derive the vapor-pressure coefficients and the gas-diffusion coefficients at 25 and 35ºC, linear regressions of literature data given at various temperatures (Mato and Cimavilla, 1983; Besley and Bottomley, 1974; Ambrose and Sprake, 1970; Nagata and Hasegawa, 1970; O'Connell *et al.*, 1969; Lugg, 1968; Arnikar *et al.*, 1967; Polak and Mertl, 1965, Bridgeman and Aldrich, 1964; Ibrahim and Kuloor, 1961; Altshuller and Cohen, 1960; Crider, 1956; Nelson, 1956; Schwertz and Brow, 1951; Fairbanks and Wilke, 1950; Kretschmer and Wiebe, 1949; Hippenmeyer, 1949; Gilliland, 1934) were calculated (Tables 2, 3) (Clausen *et al.*, 2011).

Considering the degree of precision of the diffusion coefficients required, the literature data for molecular and effective diffusion coefficients of water in smectites turned out to be insufficiently reliable for the needed simulations. The multi-scale models presume a dependence of the effective diffusion coefficient on the porosity, the number of lamellae per stack, and the relative volatile coverage, but accurate calculations remain prone to error; both the measured and computed molecular diffusion coefficients, as well as tortuosity models, are not accurate enough to be used in these multi-scale models for predictions. For these reasons a variety of different values was used for the effective diffusion coefficients in the present finite-element simulations.

Table 3. Average gas-diffusion coefficients of the volatiles.

Gas mixture	Temperature (ºC)	Average diffusion coefficient (10^{-5} m^2/s)
Ethanol/air	35	1.24
Ethyl acetate/air	35	0.92
Toluene/air	35	0.95
Water/nitrogen	35	2.64
Water/air	35	2.87
Water/nitrogen	25	2.47
Water/air	25	2.71

https://doi.org/10.1346/CCMN.2013.0610414 Published online by Cambridge University Press

Analytical model for isothermal rate of desorption

A semi-analytical model was used for comparison with experimental measurements (Clausen *et al.*, 2011). It describes the dependency of the rate of desorption of volatiles, $R(c)$, on the local instantaneous equilibrium gas-phase concentration of volatile at the surface of the sample, c, the carrier-gas flow rate, F, the temperature, T, and the system constants for the present experimental set-up (equations 3 and 4).

$$R(c) = \frac{-B + \sqrt{B^2 - 4AC}}{2A} \quad (3)$$

with

$$A = \frac{\mathrm{k}Th}{S_0 D_{\mathrm{gas}}}$$
$$B = \frac{\mathrm{k}ThF}{S_0 D_{\mathrm{gas}}} - c\mathrm{k}T + p_{\mathrm{tot}} \quad (4)$$
$$C = -c\mathrm{k}TF$$

where S_0 is the surface area of the cylindrical crucible, D_{gas} is the gas-phase diffusion coefficient, k is Boltzmann's constant, p_{tot} is the total pressure in the instrumentation, and h is the height of the crucible. The gas-phase concentration $c(\theta)$ is a function of the amount of volatile sorbed (or coverage) θ. The function $c(\theta)$ refers to the desorption branch of the equilibrium sorption isotherm.

RESULTS AND INTERPRETATION

Water equilibrium desorption isotherms

The equilibrium desorption isotherms of water onto (Na^+-rich) montmorillonite, Ca^{2+}-exchanged montmorillonite, PHTMA-exchanged montmorillonite, and HTMA-exchanged montmorillonite (Figure 1) revealed differences that are attributable to changes in the interaction between water and the interlayer cations. For a given gas-phase concentration, the amount of water sorbed by the different montmorillonite decreased in the following order: Ca^{2+}-exchanged montmorillonite > (Na^+-rich) montmorillonite > PHTMA-exchanged montmorillonite ≈ HTMA-exchanged montmorillonite. In addition, the isotherms of the Ca^{2+}-exchanged montmorillonite and (Na^+-rich) montmorillonite (inorganic cations) showed a two-step behavior, whereas the curves of the montmorillonite exchanged with the organic cations had a single step. At high gas-phase concentration, the amount of water sorbed on the Ca^{2+}-exchanged montmorillonite was comparable to (Na^+-rich) montmorillonite, and twice as large as the organic cations-exchanged montmorillonites.

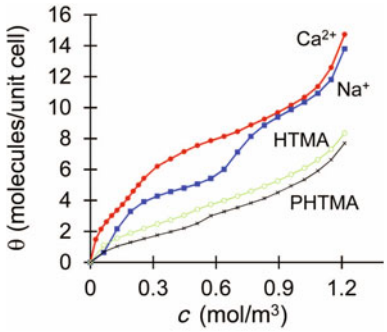

Figure 1. Equilibrium desorption isotherms of water at 25ºC on Ca^{2+}-exchanged montmorillonite, Na^+-rich montmorillonite, PHTMA-exchanged montmorillonite, and HTMA-exchanged montmorillonite. The figure represents the water coverage, θ, as a function of the gas phase concentration, c.

The differences observed in the measured equilibrium desorption isotherms at low and intermediate water coverage were attributed to differences in the strength of interaction between the interlayer cations and the water molecules. The affinity of water to Ca^{2+} and to Na^+ is sufficiently high for the respective interlayer cations to be fully hydrated and possibly form two water layers. The larger amount of water sorbed on the Ca^{2+}-exchanged montmorillonite, compared with the (Na^+-rich) montmorillonite, can be related to the greater affinity of water to Ca^{2+} than to Na^+. In turn, the affinity of water to the organic cations is not great enough to produce multiple water-layers.

From the numerical method and the analytical model, the equilibrium desorption isotherms of water from the montmorillonite are expected to be reflected in the curves of the rate of desorption. Ignoring effective diffusion effects in the sample to a first approximation, the use of equation 3 leads to the following trend for the rate of desorption: Ca^{2+}-exchanged montmorillonite > (Na^+-rich) montmorillonite > PHTMA-exchanged montmorillonite ≈ HTMA-exchanged montmorillonite

Rate of desorption of water from the ion-exchanged montmorillonite

The isothermal rate of desorption of water from cylindrical samples of the Na^+-rich, Ca^{2+}-exchanged, PHTMA-exchanged, and HTMA-exchanged montmorillonites was determined (Figure 2a) and compared to the finite-element calculation to derive the contributions of the equilibrium desorption isotherms to the rate of desorption. The experimental data of the isothermal rate showed the same behavior as the corresponding equilibrium desorption isotherms (Figure 1). This was also observed for the rate of desorption calculated with equation 3 (Figure 2b), and the finite-element calculations performed assuming constant effective diffusion coefficients of 2.3×10^{-9} m^2/s (Figure 2c) and 5×10^{-10} m^2/s inside the sample (Figure 2d). Comparing the calculations and the experimental data suggested that measured rates of desorption are

https://doi.org/10.1346/CCMN.2013.0610414 Published online by Cambridge University Press

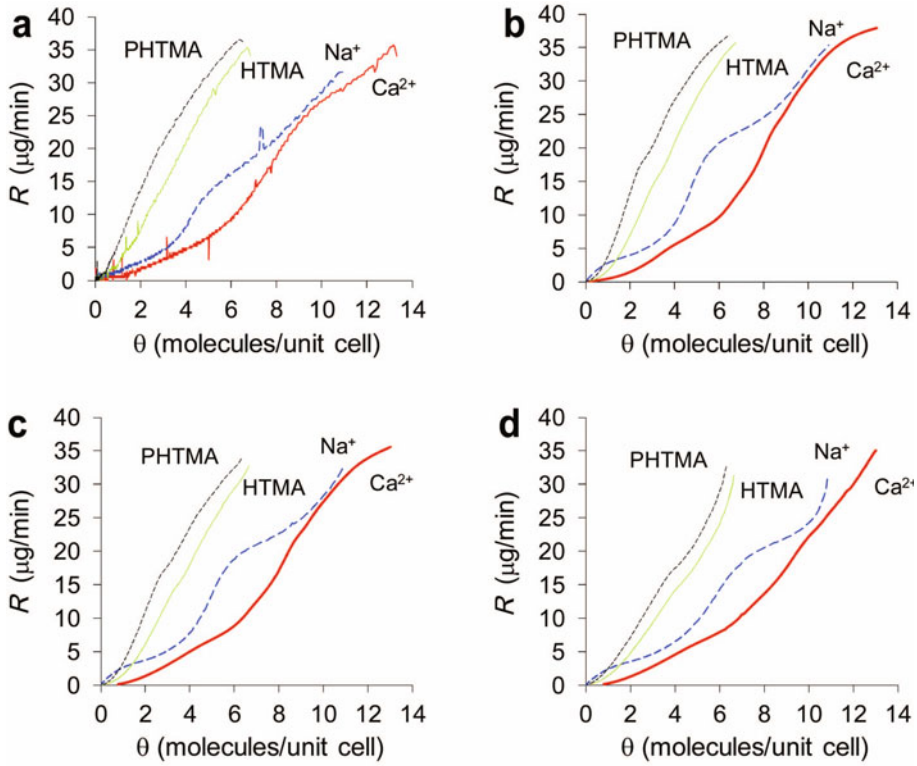

Figure 2. Desorption of water from Ca^{2+}-exchanged montmorillonite, Na^{+}-rich montmorillonite, PHTMA-exchanged montmorillonite, and HTMA-exchanged montmorillonite. Rate of desorption, R, as a function of the coverage, θ: (a) measured values; (b) semi-analytical calculations using equation 3; (c) finite-element calculations using a constant effective diffusion coefficient inside the sample of 2.3×10^{-9} m^2/s; (d) finite element calculations using a constant effective diffusion coefficient inside the sample of 5×10^{-10} m^2/s.

relatively insensitive to diffusion effects inside the sample at intermediate and high water coverage, although the behavior at low water coverage for the (Na^{+}-rich) montmorillonite did suggest that diffusion inside the sample plays a more significant role. At this stage of the desorption process, the difference in porosity, tortuosity, and molecular diffusion between the montmorillonite ion-exchanged with the various interlayer cations may influence the effective diffusion of water and, therefore, the rate of desorption. Indeed, a decrease in the value of the effective diffusion coefficient in the sample leads to a decrease in the coverage of water at the surface of the montmorillonite sample, owing to an increased coverage gradient (*i.e.* change in water concentration inside the sample) within the montmorillonite sample. Following equation 3, this can lead to a decrease in the rate of desorption.

Enthalpy of vaporization for the desorption of water from the ion-exchanged montmorillonite

The enthalpy of vaporization of water from cylindrical samples of the Na^{+}-rich, Ca^{2+}-exchanged, PHTMA-exchanged, and HTMA-exchanged montmorillonites was derived from the experimental data of the rate of desorption (Figure 3). The experimental data were consistent with the behavior of the corresponding equilibrium desorption isotherms (Figure 1). At high water coverage, the rate of desorption of water from the montmorillonite samples was equal to that of bulk water, with an enthalpy of vaporization of ~44 kJ/mol, which is equal to the enthalpy of vaporization of bulk water. As the water content decreases, the (Na^{+}-rich) and Ca^{2+}-exchanged montmorillonites showed two pronounced steps in the enthalpy of vaporization, whereas the PHTMA-exchanged and HTMA-exchanged montmorillonites showed a steady increase from 44 kJ/mol. Moreover, the second step in the enthalpy of vaporization for the Ca^{2+}-exchanged montmorillonite was considerably larger, ~2 kJ/mol, than that for the (Na^{+}-rich) montmorillonite, and, thus, a greater enthalpy of vaporization at 10% water coverage for the Ca^{2+}-exchanged montmorillonite was expected from the greater affinity of calcium to water.

The data confirmed, therefore, the trend that the rates of desorption of water from the ion-exchanged montmorillonite samples follows the curve of the equilibrium desorption isotherms. This behavior is characterized by a transition from a state comparable to that of bulk water to a state where the water interacts primarily with the interlayer cations.

https://doi.org/10.1346/CCMN.2013.0610414 Published online by Cambridge University Press

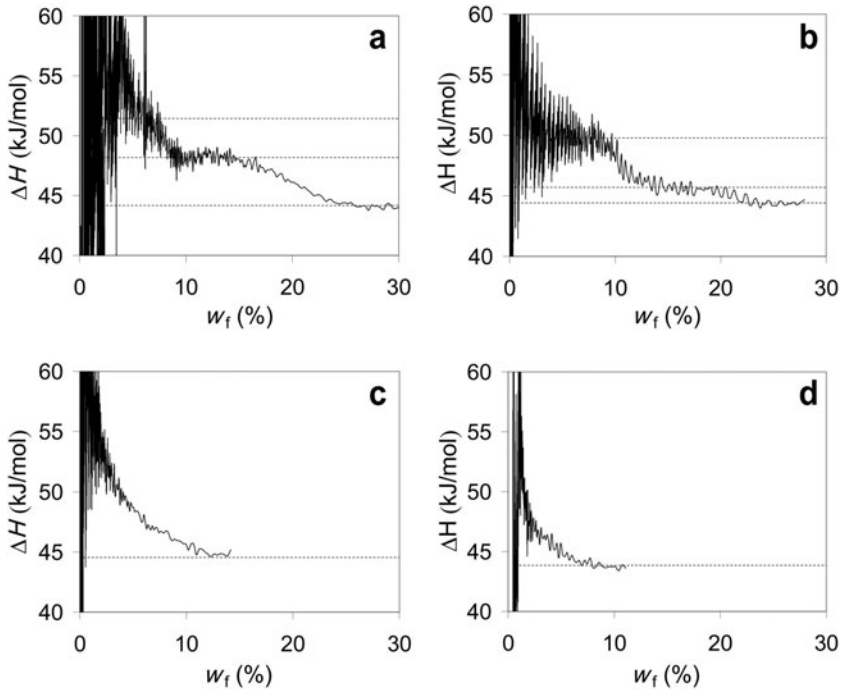

Figure 3. Measured heat of vaporization, δH, of water as a function of the water coverage, W_f, on: (a) Ca^{2+}-exchanged montmorillonite; (b) Na^{+}-rich montmorillonite; (c) PHTMA-exchanged montmorillonite; and (d) HTMA-exchanged montmorillonite.

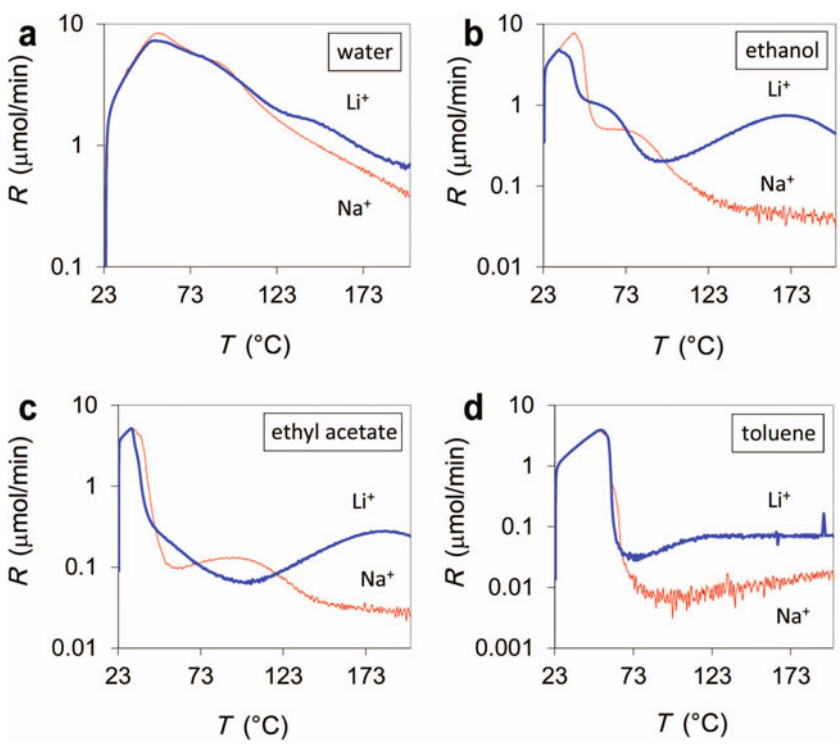

Figure 4. Temperature-ramp measurements for the desorption of 5 μL droplets of: (a) water; (b) ethanol; (c) ethyl acetate; and (d) toluene deposited on cylindrical samples of Na^{+}-rich and Li^{+}-exchanged montmorillonite. Rate of desorption, R, as a function of the temperature, T. The curves shown are averages of the duplicate measurements.

https://doi.org/10.1346/CCMN.2013.0610414 Published online by Cambridge University Press

Temperature-ramp desorption of water, ethanol, ethyl acetate, and toluene by the (Na^+-rich) and Li^+-exchanged montmorillonite

The observations that the sorbed water mainly interacts with the interlayer cations led to speculation about whether molecules of different polarities also interact predominantly with the interlayer cation. Desorption measurements of four volatiles (water, ethanol, ethyl acetate, and toluene) from the (Na^+-rich) montmorillonite were compared with desorption measurements of the same volatiles from the Li^+-exchanged montmorillonite. Due to the greater electric field strength of Li^+ as compared to Na^+, the interactions were expected to be stronger with the Li^+-exchanged montmorillonite with the volatiles, as observed previously for water equilibrated at various relative humidities (Hendricks *et al.*, 1940; Zabat and Van Damme, 2000).

In these experiments, 5 μL of the volatile liquids were deposited on cylindrical samples of the Li^+-exchanged and (Na^+-rich) montmorillonite, and the dynamic desorption was studied by temperature-ramp measurements from 23ºC to 200ºC (Figure 4). A shift of the evaporation-rate peak to higher temperatures suggests greater retention and stronger interactions with the montmorillonite. The temperatures at which the last peaks appeared for the four volatiles were ordered as

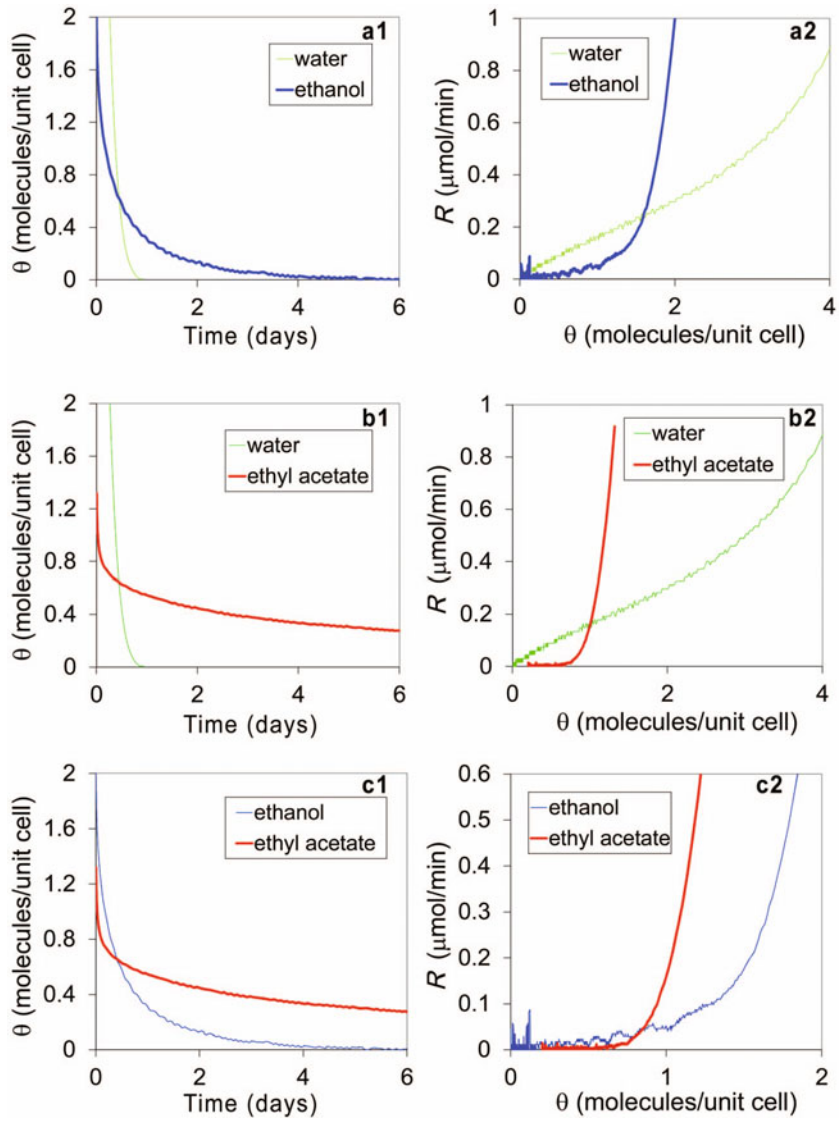

Figure 5. Measured isothermal desorption of volatiles from cylindrical samples of Na^+-rich montmorillonite at 35ºC: (a1, a2) water and ethanol; (b1, b2) water and ethyl acetate; (c1, c2) ethanol and ethyl acetate. Left: Coverage, θ, as a function of time; right: rate of desorption, *R*, as a function of coverage.

https://doi.org/10.1346/CCMN.2013.0610414 Published online by Cambridge University Press

follows: toluene < water < ethanol < ethyl acetate. This trend correlates with the trend of the affinity of the volatiles for the interlayer cation (Clausen *et al.*, 2009a).

All four volatiles showed a pronounced shift for the Li^+-exchanged montmorillonite compared to the (Na^+-rich) montmorillonite, and, thus, the stronger interactions by the Li^+-exchanged montmorillonite suggest that sorption is mediated by the interlayer cations. This effect was particularly marked for ethanol and ethyl acetate (Figure 4b, 4c), but less pronounced for toluene and water (Figure 4a, 4d). The small amount of toluene molecules sorbed and released was due to their low interaction strength with the interlayer cation (Clausen *et al.*, 2009a). In the case of water, the amounts are especially large. The peak attributed to the water molecules bound to the interlayer cation might be affected by the large peak attributed to bulk-like water (*i.e.* water regions with properties close to that of the bulk liquid) that is sorbed in large amounts due to the macroscopic swelling of the sample.

Isothermal rate of desorption of volatiles from the (Na^+-rich) montmorillonite

This section presents studies of the isothermal rate of desorption of various volatiles from the (Na+-rich) montmorillonite. The results are compared with previously obtained data of equilibrium desorption isotherms (Clausen *et al.*, 2009b). The different volatiles (water, ethanol, ethyl acetate, and toluene) were adsorbed on (Na^+-rich) montmorillonite at 0.95 activity (*i.e.* the ratio between the actual equilibrium vapor pressure of the volatile and the saturated vapor pressure of the volatile) and desorbed at 35ºC over up to 7 days under pure nitrogen.

In general, the isotherms showed clearly two regimes of desorption rates. The initial desorption rates, referring to a large degree of coverage, correlated with the evaporation rate of the bulk liquids: ethyl acetate > ethanol > water > toluene. At this coverage, the desorption behavior was dominated by volatile–volatile interactions. Below a certain degree of surface coverage, however, a pronounced influence by the surface itself was observed.

Analyzing the rate of desorption of water, ethanol, and ethyl acetate at low coverage (Figure 5) found that the trend in the rates of desorption correlated with the trend of the strengths of interaction between the volatiles and the interlayer cation. This suggests that the differences in the rates of desorption observed at low coverage between the curves were mainly due to differences in the strengths of interaction between the volatiles and the interlayer cation. The transition from a bulk-liquid behavior to a surface-interaction behavior results in a crossing between the desorption curves. The same crossing behavior was observed between the respective equilibrium desorption isotherms. The experimental results of the rates of desorption are in agreement with the calculations (Figure 6) obtained using equation 3 and the corresponding equilibrium desorption isotherm at 35ºC. Note that the calculation using equation 3 does

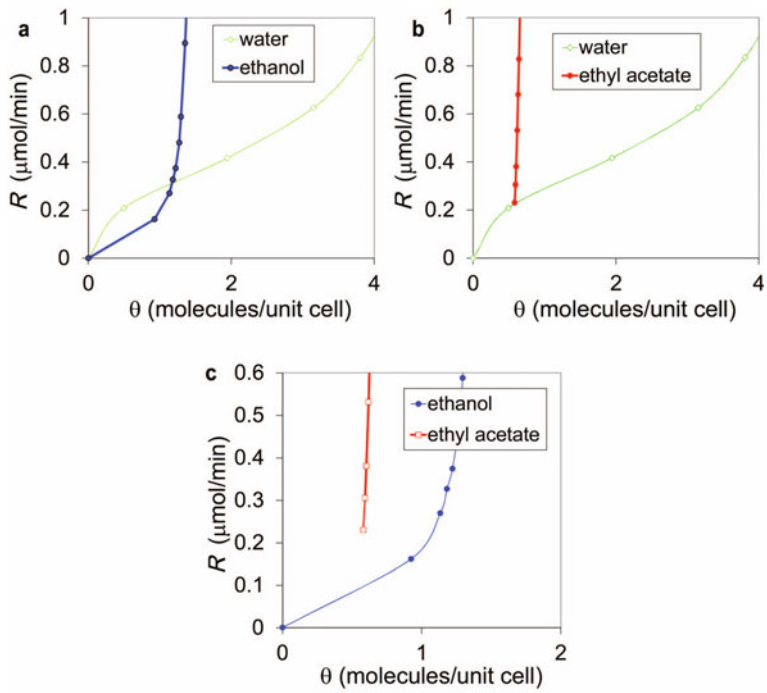

Figure 6. Calculated rate of desorption, *R*, of volatiles from cylindrical samples of Na^+-rich montmorillonite at 35ºC (equation 3): (a) water and ethanol; (b) water and ethyl acetate; and (c) ethanol and ethyl acetate.

https://doi.org/10.1346/CCMN.2013.0610414 Published online by Cambridge University Press

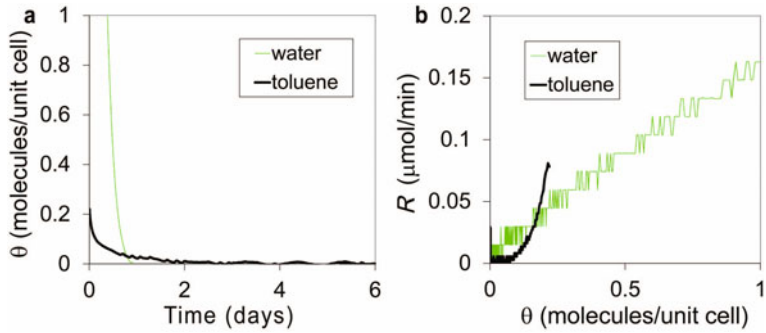

Figure 7. Desorption of water and toluene from cylindrical samples of Na^+-rich montmorillonite at 35ºC: (a) coverage, θ, as a function of time; (b) rate of desorption, *R*, as a function of coverage, θ.

not take into account diffusion effects inside the sample. Diffusion effects inside the montmorillonite are, therefore, deemed irrelevant in explaining the differences observed under these conditions.

When comparing toluene and water at low degrees of coverage, the lower rate of desorption of toluene compared to water cannot be explained by differences in the affinity for the interlayer cation, because the strength of interaction of water with the interlayer cation is greater than that of toluene (Figure 7). The calculation of the desorption of toluene from the (Na+-rich) montmorillonite (Figure 8) obtained using equation 3, and the corresponding equilibrium desorption isotherm at 35ºC, shows that without diffusion effects inside the sample the rate of desorption of toluene would be greater than that of water. This suggests the effective diffusion of toluene inside the sample to be significantly lower than that of water. Indeed, previous studies of Ca^{2+}- and Cu^{2+}-exchanged montmorillonite (Shih *et al.*, 2004; Chang *et al.*, 2003) suggested that a residual fraction of toluene seems to resist desorption. Another study of montmorillonites ion-exchanged with five different cations (K^+, Na^+, Ca^+, Mg^{2+}, Fe^{3+}) supports the conclusion that recalcitrant fractions may be stored in clay particle micro-aggregates (Steinberg *et al.*, 1994). In the present case, some toluene molecules could possibly become trapped in the (Na^+-rich) montmorillonite sample, after equilibration of the (Na^+-rich) montmorillonite with toluene prior to desorption measurements.

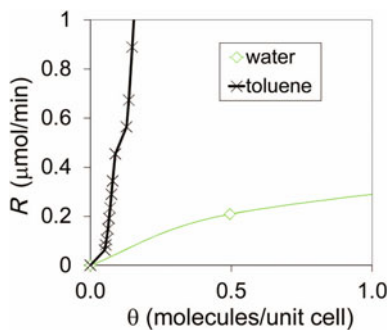

Figure 8. Calculated rate of desorption, *R*, of water and toluene from cylindrical samples of Na^+-rich montmorillonite at 35ºC using equation 3.

CONCLUSIONS

Results for the rate of desorption of water from (Na^+-rich) montmorillonite, Ca^{2+}-exchanged montmorillonite, PHTMA-exchanged montmorillonite, and HTMA-exchanged montmorillonite, and for the rate of desorption of water, ethanol, ethyl acetate, and toluene from (Na^+-rich) and Li^+-exchanged montmorillonite, were presented. Analysis of the experimental and theoretical results showed the rate of desorption to be strongly related to the equilibrium desorption isotherms of the volatiles on the montmorillonite. With a large degree of coverage by the volatile, the state was similar to that of the bulk liquid, so that the type of interlayer cations had no effect on the initial rate of desorption. While the degree of coverage decreased at the sample surface, the rate of desorption followed the curves of the equilibrium desorption isotherms. At low volatile coverage, the rate of desorption was strongly influenced by the strength of interaction between the volatile and the interlayer cation. In addition, diffusion played a role by decreasing the coverage at the sample surface. In particular, the rate of desorption of toluene decreased strongly despite its weak interaction with the interlayer cation.

The accurate determination of the effective diffusion coefficient of volatiles in smectites as a function of vapor pressure and its connection to the change in porosity, tortuosity, and molecular diffusion remain challenging both experimentally and numerically. Future research in this direction may provide significant further insights into the mechanisms of desorption of volatiles from smectites.

ACKNOWLEDGMENTS

This study was supported financially by the Nestlé Research Center (NESTEC, Switzerland).

https://doi.org/10.1346/CCMN.2013.0610414 Published online by Cambridge University Press

REFERENCES

Altshuller, A.P. and Cohen, I.R. (1960) Application of diffusion cells to the production of known concentrations of gaseous hydrocarbons. *Analytical Chemistry*, **32**, 802–810

Ambrose, D. and Sprake, C.H.S. (1970) Thermodynamic properties of organic oxygen compounds. XXV. Vapor pressures and normal boiling temperatures of aliphatic alcohols. *Journal of Chemical Thermodynamics*, **2**, 631–645

Arnikar, H.J., Rao, T.S., and Karmarkar, K.H. (1967) Electrodeless discharge as detector in gas chromatography III. Study of inter-diffusion of gases. *International Journal of Electronics*, **22**, 381–385.

Arocha, M.A., Jackman, A.P., and McCoy, B.J. (1996) Adsorption kinetics of toluene on soil agglomerates: Soil as a biporous sorbent. *Environmental Science & Technology*, **30**, 1500–1507.

Bérend, I., Cases, J.M., François, M., Uriot, J.P., Michot, L., Masion, A., and Thomas, F. (1995) Mechanism of adsorption and desorption of water vapor by homoionic montmorillonites: 2. The Li^+, Na^+, K^+, Rb^+, and Cs^+-exchanged forms. *Clays and Clay Minerals*, **43**, 324–336.

Besley, L.M. and Bottomley, G.A. (1974) Vapour pressure of toluene from 273.15 to 298.15 K. *Journal of Chemical Thermodynamics*, **6**, 577–580.

Bharadwaj, R.K. (2001) Modeling the barrier properties of polymer-layered silicate nanocomposites. *Macromolecules*, **34**, 9189–9192.

Boek, E.S., Coveney, P.V., and Skipper, N.T. (1995) Monte Carlo molecular modeling studies of hydrated Li-, Na-, and K-smectites: Understanding the role of potassium as a clay swelling inhibitor. *Journal of the American Chemical Society*, **117**, 12608–12607.

Bourg, I.C., Sposito, G., and Bourg, A.C.M. (2006) Tracer diffusion in compacted, water-saturated bentonite. *Clays and Clay Minerals*, **54**, 363–374.

Bray, H.J. and Redfern, S.A.T. (1999) Kinetics of dehydration of Ca-montmorillonite. *Physics and Chemistry of Minerals*, **26**, 591–600.

Bridgeman, O.C. and Aldrich, E.W. (1964) Vapor pressure tables for water. *Journal of Heat Transfer*, **86**, 279–286.

Cases, J.M., Bérend, I., François, M., Uriot, J.P., Michot, L.J., and Thomas, F. (1997) Mechanism of adsorption and desorption of water vapor by homoionic montmorillonite; 3. The Mg^{2+}, Ca^{2+}, and Ba^{3+} exchanged forms. *Clays and Clay Minerals*, **45**, 8–22.

Cebula, D.J., Thomas, R.K., and White, J.W. (1981) Diffusion of water in Li-montmorillonite studied by quasielastic neutron scattering. *Clays and Clay Minerals*, **29**, 241–248.

Chang, F.-R.C., Skipper, N.T., and Sposito, G. (1995) Computer simulation of interlayer molecular structure in sodium montmorillonite hydrates. *Langmuir*, **11**, 2734–2741.

Chang, M.-L., Wu, S.-C., Chen P.-J., and Cheng, S.-C. (2003) Infrared investigation of the sequestration of toluene vapor on clay minerals. *Environmental Toxicology and Chemistry*, **22**, 1956–1962.

Clausen, P., Andreoni, W., Curioni, A., and Hughes, E., (2009a) Adsorption of low-molecular-weight molecules on a dry clay surface: An ab initio study. *Journal of Physical Chemistry C*, **113**, 12293–12300.

Clausen, P., Signorelli, M., Schreiber, A., Hughes, E., Plummer, J.G.P., Fessas, D., Schiraldi, A., and Månson, E.J.A. (2009b) Equilibrium desorption isotherms of water, ethanol, ethyl acetate, and toluene on a sodium smectite clay. *Journal of Thermal Analysis and Calorimetry*, **98**, 833–841.

Clausen, P., Watzke, B., Hughes, E., Plummer, J.G.P., and Månson, E.J.A. (2011) Evaporation kinetics of volatile liquids and release kinetics of water from a smectite clay: Comparison between experiments and finite element calculations. *International Journal of Engineering Science*, **49**, 1125–1140.

Crider, W.L. (1956) The use of diffusion coefficients in the measurement of vapour pressure. *Journal of the American Chemical Society*, **78**, 924–925.

Duval, F.P., Porion, P., Faugere, A.-M., and Van Damme, H. (1999) Microscale and macroscale diffusion of water in colloidal gels. A pulsed field gradient and NMR imaging investigation. *Journal of Physical Chemistry*, **103**, 5730–5735.

El-Nokaly, M.A., Piatt, D.M., and Charpentier, B.A. (1993) *Polymeric Delivery Systems: Properties and Applications.* ACS Symposium Series, American Chemical Society.

Fairbanks, D.F. and Wilke, C.R. (1950) Diffusion coefficients in multicomponent gas mixtures. *Industrial and Engineering Chemistry*, **42**, 471–475.

Ferrage, E., Lanson, B., Sakharov, B.A., and Drits, V.A. (2005) Investigation of smectite hydration properties by modeling experimental X-ray diffraction patterns: Part I. Montmorillonite hydration properties. *American Mineralogist*, **90**, 1358–1374.

Frezzotti, A., Gibelli, L., and Lorenzani, S. (2005) Mean field kinetic theory description of evaporation of a fluid into vacuum. *Physics of Fluids*, **17**, 012102, (doi: 10.1063/1.1824111).

Fujii, N., Ichikawa, Y., Katsuyuki, K., Suzuki, S., and Kitayama, K. (2003) Micro-structure of bentonite clay and diffusion coefficient given by multiscale homogeneization analysis. *Materials Science Research International*, **9**, 117–124

Gilliland, E.R. (1934) Diffusion coefficients in gaseous systems. *Industrial and Engineering Chemistry*, **26**, 681–685

Girard, F., Antoni, M., Faure, S., and Steinchen, A. (2006) Evaporation and marangoni driven convection in small heated water droplets. *Langmuir*, **22**, 11085–11091.

Grismer, M.E. (1987a) Kinetics of water vapor adsorption on soils. *Soil Science*, **143**, 367–371.

Grismer, M.E. (1987b) Vapor adsorption kinetics and vapor diffusivity. *Soil Science*, **144**, 1–5.

Hendricks, S.B., Nelson, R.A., and Alexandre, M. (1940) Hydration mechanism of the clay mineral montmorillonite saturated with various cations. *Journal of the American Chemical Society*, **62**, 1457–1464.

Hensen, E.J.M. and Smit, B. (2002) Why clays swell. *Journal of Physical Chemistry B*, **106**, 12664–12667.

Hippenmeyer, B. (1949) Die Diffusion von Wasserdampf in Wasserstoff, Stickstoff und deren Gemischen. *Angewandte Physik*, **1**, 549–557.

Ibrahim, S.H. and Kuloor, N.R. (1961) Diffusion in binary gas system. *British Chemical Engineering*, **6**, 862–863.

Keyes, B.R. and Silicox, G.D. (1994) Fundamental study of the thermal desorption of toluene from montmorillonite clay particles. *Environmental Science & Technology*, **28**, 840–849.

Kraehenbuehl, F., Stoeckli, H.F., Brunner, F., Kahr, G., and Müller-Vonmoos, M. (1987) Study of the water-bentonite-system by vapour adsorption, immersion calorimetry and X-ray techniques, I. Micropore volumes and internal surface areas, following Dubinin's theory. *Clay Minerals*, 22, 1–9.

Kretschmer, C.B. and Wiebe, R. (1949) Liquid-vapor equilibrium of ethanol-toluene solutions. *Journal of the American Chemical Society*, **71**, 1793–1797.

Landau, L.D. and Lifschitz, E.M. (1987) *Fluid Mechanics*. 2nd edition, Pergamon Press, Oxford, UK.

Lugg, G.A. (1968) Diffusion coefficients of some organic and

other vapors in air. *Analytical Chemistry*, **40**, 1072–1077.
Lusti, H.R., Gusev, A.A., and Guseva, O. (2004) The influence of platelet disorientation on the barrier properties of composites: a numerical study. *Modelling and Simulation in Materials Science and Engineering*, **12**, 1201–1207.
Malikova, N., Cadene, A., and Marry, V. (2006) Diffusion of water in clays on the microscopic scale: modeling and experiment. *Journal of Physical Chemistry B*, **110**, 3206–3214.
Marry, V., Malikova, N., Cadène, A., Dubois, E., Durand-Vidal, A., Turq, P., Breu, J., Longeville, S., and Zanotti, J.-M. (2008) Water diffusion in a synthetic hectorite by neutron scattering – beyond the isotropic translation model. *Journal of Physics: Condensed Matter*, **20**, 104205–104215.
Mato, F. and Cimavilla, J.M. (1983) Determinacion de coeficientes binarios de difusion en fase gaseosa mediante el metodo experimental de Stefan. *Anales De Quimica*, **79**, 445–448.
Meier, L.P. and Kahr, G. (1999) Determination of the cation exchange capacity (CEC) of clay minerals using the complexes of copper(II) ions with triethylenetetramine and tetraethylenepentamine. *Clays and Clay Minerals*, **47**, 386–388.
Michot, L.J., Bihannic, I., Pelletier, M., Rinnert, E., and Robert, J.-L. (2005) Hydration and swelling of synthetic Na-saponites: Influence of layer charge. *American Mineralogist*, **90**, 166–172.
Morodome, S. and Kawamura, K. (2009) Swelling behavior of Na- and Ca-montmorillonite up to 150ºC by in situ X-ray diffraction experiments. *Clays and Clay Minerals*, **57**, 150–160.
Morrissey, F.A. and Grismer, M.E. (1999) Kinetics of volatile organic compound sorption/desorption on clay minerals. *Journal of Contaminant Hydrology*, **36**, 291–312.
Nagata, I. and Hasegawa, T. (1970) Gaseous interdiffusion coefficients. *Journal of Chemical Engineering of Japan*, **3**, 143–145.
Nakashima, Y. (2000a) Effects of clay fraction and temperature on the H_2O self-diffusivity in hectorite gel: A pulsed-field-gradient spin-echo nuclear magnetic resonance study. *Clays and Clay Minerals*, **48**, 603–609.
Nakashima, Y. (2000b) Pulsed field gradient proton NMR study of the self-diffusion of H_2O in montmorillonite gel: effects of temperature and water fraction. *American Mineralogist*, **85**, 132–138.
Nakashima, Y. (2002) Diffusion of H_2O and I- in expandable mica and montmorillonite gels: contribution of bound H_2O. *Clays and Clay Minerals*, **50**, 1–10.
Nakashima, Y. (2003) Diffusion of H_2O in smectite gels: obstruction effects of bound H_2O layers. *Clays and Clay Minerals*, **51**, 9–22.
Nakashima, Y. (2006) H_2O self-diffusion coefficient of water rich MX-80 bentonite gels. *Clay Minerals*, **41**, 659–668.
Navier, C.L.M.H. (1822) Mémoire sur les lois du mouvement des fluides. *Mémoires de l'Académie des Sciences de l'Institut de France*, **6**, 389–440.
Nelson, E.T. (1956) The measurement of vapour diffusivities in coal-gas and some common gases. *Journal of Applied Chemistry*, **6**, 286–292.
Norrish, K. (1954) The swelling of montmorillonite. *Discussions of the Faraday Society*, **18**, 120–134.
O'Connell, J.P., Gillespie, M.D., Krostek, W.D., and Prausnitz, J.M. (1969) Diffusivities of water in nonpolar gases. *Journal of Chemical Physics*, **73**, 2000–2004.
Ochs, M., Lothenbach, B., Shibata, M., and Mikazu, Y. (2004) Thermodynamic modeling and sensitivity analysis of pore-water chemistry in compacted bentonite. *Physics and Chemistry of the Earth*, **29**, 129–136.
Poinsignon, J., Estrade-Szwarckopf, H., Conard, J., and Dianoux, A.J. (1989) Structure and dynamics of intercalated water in clay minerals. *Physica B: Physics of Condensed Matter*, **156-157**, 140–144.
Polak, J. and Mertl, I. (1965) Saturated vapour pressure of methyl acetate, ethyl acetate, n-propyl acetate, methyl propionate, and ethyl propionate. *Collection of Czechoslovak Chemical Communications*, **30**, 3526–3528.
Polubesova, T., Rytwo, G., Nir, S., Serban, C., and Margulies, L. (1997) Adsorption of benzyltrimethylammonium and benzyltriethylammonium on montmorillonite: Experimental studies and model calculations. *Clays and Clay Minerals*, **45**, 834–841.
Sato, H. and Suzuki, S. (2003) Fundamental study on the effect of an orientation of clay particles on diffusion pathway in compacted bentonite. *Applied Clay Science*, **23**, 51–60.
Schwertz, F.A. and Brow, J.E. (1951) Diffusivity of water vapor in some common gases. *Journal of Chemical Physics*, **19**, 640–646.
Salles, F., Beurroies, I., Bildstein, O., Jullien, M., Raynal, J., Denoyel, R., and Van Damme, H. (2008) A calorimetric study of mesoscopic swelling and hydration sequence in solid Na-montmorillonite. *Applied Clay Science*, **39**, 186–201.
Shih, Y.-H. and Wu, S.-C. (2004) Kinetics of toluene sorption and desorption in Ca- and Cu-montmorillonites investigated with Fourier transform infrared spectroscopy under two different levels of humidity. *Environmental Toxicology and Chemistry*, **23**, 2061–2067.
Siepmann, J., Ainaoui, A., Vergnaud, J.M., and Bodmeier, R. (1998) Calculation of the dimensions of drug-polymer devices based on diffusion parameters. *Journal of Pharmaceutical Sciences*, **87**, 827–832.
Skipper, N.T., Lock, P.A., Titiloye, J.O., and Swenson, J. (2006) The structure and dynamics of 2-dimensional fluids in swelling clays. *Chemical Geology*, **230**, 182–196.
Suzuki, A., Sato, H., Ishidera, T., and Fujii, N. (2004) Study on anisotropy of effective diffusion coefficient and activation energy for deuterated water in compacted sodium bentonite. *Journal of Contaminant Hydrology*, **68**, 23–37.
Steinberg, S., Fairley, J.P., and Kreamer, D. (1994) Slow vapor-phase desorption of toluene from several ion-exchanged monmorillonites. *Journal of Soil Contamination*, **3**, 249–264.
Swenson, J., Bergman, R., and Howells, W.S. (2000) Quasielastic neutron scattering of two-dimensional water in a vermiculite clay. *Journal of Chemical Physics*, **113**, 2873–2879.
Tambach, T.J., Bohuis, P.G., Hensen, J.M., and Smit, B. (2006) Hysteresis in clay swelling induced by hydrogen bonding: accurate prediction of swelling states. *Langmuir*, **22**, 1223–1234.
Tamura, K., Yamada, H., and Nakazawa, H. (2000) Stepwise hydration of high-quality synthetic smectite with various cations. *Clays and Clay Minerals*, **48**, 400–404.
Tuck, J.J., Hall, P.L., Hayes, M.H.B., Ross, D.K., and Poinsignon, J. (1984) Quasi-elastic neutron-scattering studies of intercalated molecules in charged-deficient layer silicates: part 1. *Journal of the Chemical Society Faraday Transaction 1: Physical Chemistry in Condensed Phases*, **80**, 309–324.
Tuck, J.J., Hall, P.L., and Hayes, M.H.B. (1985) Quasi-elastic neutron-scattering studies of intercalated molecules in charged-deficient layer silicates: Part 2. *Journal of the Chemical Society Faraday Transactions 1: Physical Chemistry in Condensed Phases*, **81**, 833–846.
Veith, S.R., Hughes, E., and Pratsinis, S.E. (2004) Restricted diffusion and release of aroma molecules from sol-gel-made porous silica particles. *Journal of Controlled Release*, **99**, 315–327.

Ward, C.A. and Fang, G. (1999) Expression for predicting liquid evaporation flux: statistical rate theory approach. *Physical Review E*, **59**, 429–439.

Zabat, M. and Van Damme, H. (2000) Evaluation of the energy barrier for dehydration of momionic (Li, Na, Cs, Mg, Ca, Ba, Alx(OH)yz^{+} and La)-montmorillonite by a differentiation method. *Clay Minerals*, **35**, 357–363.

(*Received 25 August 2011; revised 23 September 2013; Ms. 609; AE: R. Dohrmann*)